ELSEVIER

Chemical Engineering Journal 137 (2008) 664–676

Chemical Engineering Journal

www.elsevier.com/locate/cej

CFD modelling of a countercurrent staged fluidised bed

H.P. Kuo *, H.Z. Zhang, R.C. Hsu

Department of Chemical and Materials Engineering, Chang Gung University, Tao-Yuan 333, Taiwan

Received 4 July 2007; received in revised form 16 August 2007; accepted 16 August 2007

Abstract

The bed flow regimes and the hydrodynamics in a 2D countercurrent staged fluidised bed were simulated using Computation Fluid Dynamics (CFD). Based on the two-fluid theory, an Eulerian–Eulerian approach coupled with kinetic theory of granular flow (KTGF) for the solid phase was applied. The predictions were compared with the experimental results of Kuo and Cheng (2006). The calculated and experimental results both showed a non-growth flow regime, a dilute flow regime, an oscillating flow regime, a bubbling flow regime and a flooding flow regime on the perforated plate at different operating conditions. The values of the predicted pressure drop across the bed at steady state for the dilute flowing regime and the bubbling flowing regime agreed quantitatively well with the previous experimental results, although the time to reach the steady state was different. The calculated flow regime map as functions of the gas velocities and solids feeding rates agreed qualitatively with the experiments.

Keywords: Fluidisation; CFD; Eulerian–Eulerian approach; Perforated plate; Countercurrent fluidised bed; Kinetic theory of granular flow

1. Introduction

Gas–solid fluidised beds are widely applied in many industries as reactors or heat/mass transferring units because of their good heterogeneous mixing behaviour and large transferring area between the gas and solid phases. Evaluation of the performance of a fluidised bed requires a good understanding of the hydrodynamic behaviour at each flow regimes (i.e., bubbling, slugging, etc.); however, the investigation methods are limited. The non-invasive experimental techniques for the investigation of a commercial scale fluidised bed are not yet available, although the PEPT technique and the MRI technique had been applied to study the bench scale fluidised beds [1,2]. With the rapid increasing computational power, using the numerical simulation method as a fluidised bed design tool is currently a popular research topic [3–6].

Two approaches have been applied to simulate fluidised bed systems, namely the Eulerian Fluid–Lagrangian Discrete Particle (EFLDP) approach and the Eulerian Fluid–Eulerian Continuum Particle (EFECP) approach. The EFLDP approach solves the equation of motion for individual particles in the system. The particle–particle interactions and particle–fluid interactions are considered at particulate scale [7–9]. The advantage of the EFLDP approach is that the trajectory of each particle can be modelled. However, a typical fluidised bed contains a very large number of particles and an expensive computational resource is required for the EFLDP approach. Currently, a system with hundreds of thousands of 3 mm particles has been modelled; nevertheless, the diameter of the simulated column was only 15 cm in diameter and 30 cm in height [7]. It is not likely to simulate a commercial fluidised bed even using the state-of-the-art supercomputing facility through the EFLDP approach. On the other hand, the EFECP approach treats the particle assembly as a continuum. The solid phase and fluid phase are interpenetrating continua. The computational efficiency can be very effective compared to the EFLDP approach and the simulation of a large fluidised bed is possible.

The EFECP approach applied to the gas–solid fluidised bed is also known as the two-fluid theory. Two common models have been applied to the solid phase for the internal momentum transfer, namely the kinetic theory of granular flow model (KTGF) [10] and the constant viscosity model (CVM) [11]. The KTGF model seems to be more popular than the CVM model in recent years since the KTGF model considers the solid phase properties in terms of instantaneous binary particle-particle interactions and gives a more fundamental insight of the particle–particle interactions compared with the CVM model. A critical comparison between the CVM and KTGF model has been made recently by Patil et al. [5]. The EFECP approach coupled with KTGF CFD simulations has been applied to other fluidisation systems,

* Corresponding author. Tel.: +886 3 2118800x5488; fax: +886 3 2118668.
E-mail address: hpkuo@mail.cgu.edu.tw (H.P. Kuo).

1385-8947/$ – see front matter © 2007 Published by Elsevier B.V.
doi:10.1016/j.cej.2007.08.021

Table 1
KTGF theory applied to the solid phase in current study

Term	Model	Ref.
Solid pressure	$p_s = \varepsilon_s\rho_s\theta_s + 2\rho_s(1+e_{ss})\varepsilon_s^2 g_0\theta_s$ where e_{ss}, $g_{0,ss}$, and θ_s are the particle–particle restitution coefficient, the radial distribution at contact and the granular temperature of the solid phase, respectively	[24]
Solid phase radial distribution at contact	$g_0 = \left[1 - \left(\frac{\varepsilon_s}{\varepsilon_{s,max}}\right)^{\frac{1}{3}}\right]^{-1}$ where $\varepsilon_{s,max}$ is the maximum solid volume fraction of a random packing	[25]
Solid phase granular temperature conservative equation	$\frac{3}{2}\left[\frac{\partial}{\partial t}(\rho_s\varepsilon_s\theta_s) + \nabla(\rho_s\varepsilon_s\vec{u}_s\theta_s)\right] = (-p_s\bar{\bar{I}} + \bar{\bar{\tau}}_s) : \nabla\vec{u}_s + \nabla(k_{\theta_s}\nabla\theta_s) - \gamma_{\theta_s} + \phi_{gs}$ where $\bar{\bar{I}}$ is the unit tensor	[24]
Solid stress tensor	$\tau_s = -\left\{\left(\lambda_s - \frac{2}{3}\mu_s\right)(\nabla\vec{u}_s)\bar{\bar{I}} + \mu_s((\nabla\vec{u}_s) + (\nabla\vec{u}_s)^T)\right\}$ where λ_s and μ_s are the solid phase bulk viscosity and the solid phase shear viscosity, respectively	[5]
Solid phase bulk viscosity	$\lambda_s = \frac{4}{3}\varepsilon_s^2\rho_s d_p g_0(1+e_{ss})\sqrt{\frac{\theta_s}{\pi}}$	[6,24,27]
Solid phase shear viscosity	$\mu_s = \mu_{s,col} + \mu_{s,kin}$	[28]
Collisional viscosity	$\mu_{s,col} = \frac{4}{5}\varepsilon_s^2\rho_s d_p g_{0,ss}(1+e_{ss})\left(\frac{\theta_s}{\pi}\right)^{1/2}$	[28]
Kinetic viscosity	$\mu_{s,kin} = \frac{10\rho_s d_s\sqrt{\theta_s\pi}}{96(1+e_{ss})g_{0,ss}}\left[1 + \frac{4}{5}g_{0,ss}\varepsilon_s(1+e_{ss})\right]^2$	[28]
Collisional energy dissipation	$\gamma_{\theta_s} = \frac{12(1-e_{ss}^2)g_{0,ss}}{d_s\sqrt{\pi}}\rho_s\varepsilon_s^2\theta_s^{3/2}$	[10]
Fluctuating energy exchange between the gas and the solid phases[a]	$\phi_{gs} = -3K_{gs}\theta_s$	[29]

[a] The rate of production of granular temperature by gas–solids slip is neglected in this work. This is a reasonable assumption for the heavy particles used in the simulation [17,30].

including batch fluidised bed systems [5,6,12–14] and circulating fluidised bed systems [15–18], but has yet been applied to simulate the countercurrent staged fluidised bed systems. In this paper, we applied the EFECP approach coupled with KTGF CFD simulations to model a countercurrent fluidised bed system.

The diameter of the holes on the perforated plate in a countercurrent staged fluidised bed system is several times larger than the particle diameter. The particles can pass through the holes on the plate and a particle-downwards-gas-upwards countercurrent fashion is obtained. The countercurrent staged fluidised bed sys-

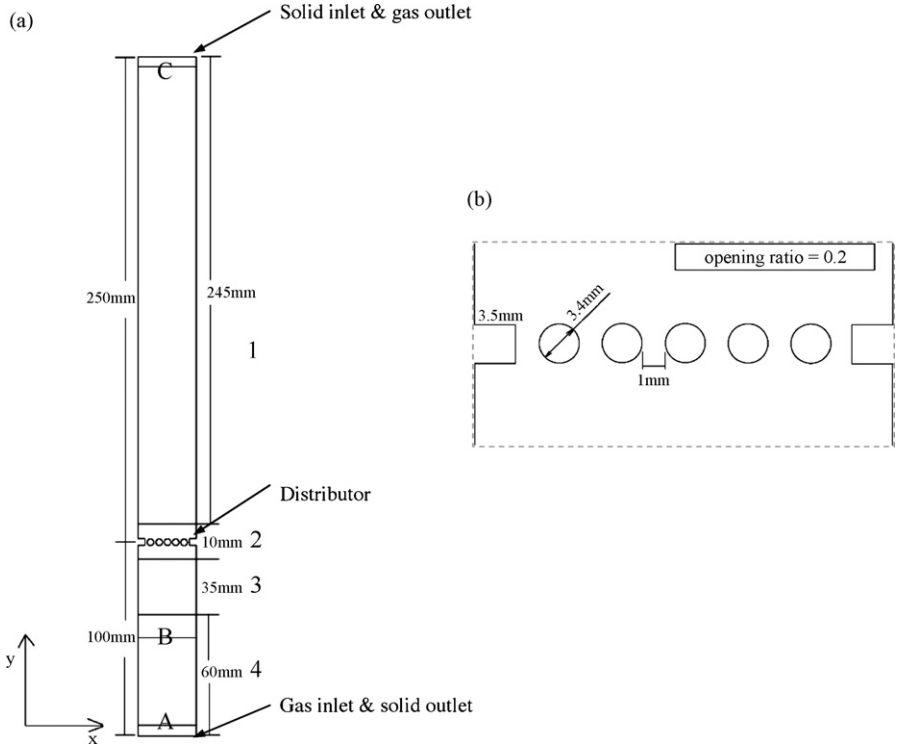

Fig. 1. (a) The schematic drawing of the simulated system; A, B and C represent the three levels showing the microscopic gas pressure and the solid mass flux values; 1, 2, 3 and 4 indicate the 4 different sections with different meshes. (b) The enlarged drawing of the 2D perforated plate.

tems found good applications in drying, heat recovery and other industrial processes [19–22]. There are several advantages for the addition of the horizontal plate(s) to the fluidising column. The plate(s) may avoid the formation of large bubbles/slugs and reduce the solids short-cut in the circulation pattern and hence narrow the particle residence time in the bed [19]. The particle residence time in the system can be adjusted by the plate numbers [20–22]. Different flow regimes have been reported in countercurrent staged fluidised bed systems at different operating parameters, including a non-growth regime, a dilute regime, an oscillating shallow bed regime, a stable bubbling regime, a slugging regime and a flooding regime [21–23]. The prediction of the stable bubbling regime of a countercurrent system is largely empirical and hence limits the popularity of this system. In current work, we initially applied the EFECP approach coupled with KTGF CFD simulations to investigate the hydrodynamics and to predict the flow regimes in a countercurrent fluidised bed with a perforated plate and the calculated results were compared with the experimental results of Kuo and Cheng [22].

2. Theory

The two-fluid theory was used to simulate the countercurrent fluidised bed. The gas and solid phases were modelled as continuous phases. The governing equations include the continuity equation and the momentum equations. The continuity equation for phase i is

$$\frac{\partial}{\partial t}(\varepsilon_i \rho_i) + \nabla(\varepsilon_i \rho_i \vec{u}_i) = 0,$$

$$i = g, s \text{ (g for gas phase and s for solid phase)} \quad (1)$$

where ε, ρ and $\vec{u}$ are the volume fraction, density and velocity for each phase, respectively.

The gas phase momentum equation is

$$\frac{\partial}{\partial t}(\varepsilon_g \rho_g \vec{u}_g) + \nabla(\varepsilon_g \rho_g \vec{u}_g \vec{u}_g) = -\varepsilon_g \nabla p + K_{sg}(\vec{u}_s - \vec{u}_g) + \nabla \bar{\bar{\tau}}_g + \varepsilon_g \rho_g \vec{g} + \varepsilon_g \rho_g \vec{F}_{vm} \quad (2)$$

The solid phase momentum equation is

$$\frac{\partial}{\partial t}(\varepsilon_s \rho_s \vec{u}_s) + \nabla(\varepsilon_s \rho_s \vec{u}_s \vec{u}_s) = -\varepsilon_s \nabla p + K_{sg}(\vec{u}_g - \vec{u}_s) + \nabla \bar{\bar{\tau}}_s - \nabla p_s + \varepsilon_s \rho_s \vec{g} + \varepsilon_s \rho_s \vec{F}_{vm} \quad (3)$$

where p, p_s, $\bar{\bar{\tau}}_g$, $\bar{\bar{\tau}}_s$, g, $\vec{F}_{vm}$ and K_{sg} are the gas pressure, the solid pressure, the gas phase stress tensor, the solid phase stress tensor, the gravitational acceleration, the virtual mass force, and the interphase momentum transfer coefficient, respectively. Because the virtual mass force term is only important for multi-phase flows where the dispersed phase density is much smaller than the continuous phase such as gas–liquid bubbly flows; therefore, the virtual mass force term was neglected in our simulations.

When the governing equations (1)–(3) are solved simultaneously with appropriate initial/boundary conditions, the

Table 2
Simulation conditions

Case	Particle phase mass flux (kg/sm^2)	Superficial gas velocity (m/s)	Initial gas turbulent energy ($\times 10^{-3}$, Nm)	Initial gas turbulent energy dissipation rate (m^2/s^3)	Particle phase feeding velocity (m/s)	Initial particle phase solids fraction ($\times 10^{-4}$)(−)	Initial particle phase granular temperature (m^2/s^2)	Flow regime
1	0.328	1.18	5.570	3.246	1.65	0.631	0.01089	Non-growth
2	2.000	0.80	2.560	1.812	1.65	3.848	0.01089	Dilute
3	0.647	1.30	6.760	3.754	1.65	1.245	0.01089	Dilute
4	0.695	1.44	8.294	4.376	1.65	1.337	0.01089	Dilute
5	1.000	1.70	11.56	5.613	1.65	1.924	0.01089	Oscillating
6	3.500	0.80	2.560	1.812	1.65	6.734	0.01089	Stable
7	2.120	1.16	5.382	3.164	1.65	4.079	0.01089	Stable
8	1.500	1.18	5.570	3.246	1.65	2.886	0.01089	Stable
9	2.924	1.18	5.570	3.246	1.65	5.626	0.01089	Stable
10	2.000	1.50	9.000	4.653	1.65	3.848	0.01089	Stable
11	4.000	1.50	9.000	4.653	1.65	7.696	0.01089	Flooding
12	6.200	1.70	11.56	5.613	1.65	11.92	0.01089	Flooding
13	6.291	1.90	14.44	6.633	1.65	12.10	0.01089	Flooding

hydrodynamic properties of the system can be obtained as a function of time. Nevertheless, the solid pressure, the solid phase stress tensors and the interphase momentum transfer coefficient in the governing equations are not directly obtained from the measurement. Therefore, the derivations of these terms are addressed in detail below based on the KTGF theory [10] summarised in Table 1.

In our computations, $\varepsilon_{s,max}$ equals to 0.55 is used to calculate the radial distribution at contact of the solid phase. Compared to the previous work of Ding and Gidaspow [24] ($\varepsilon_{s,max} = 0.6436$), Du et al. [6] ($\varepsilon_{s,max} = 0.59$) and Samuelsberg and Hjertager [27] ($\varepsilon_{s,max} = 0.65$), the maximum solid volume fraction value used is smaller in our simulations. Although the maximum random dense packing for monosized spheres is 0.637, the packing density at the onset of fluidisation is typically around 0.55 [26]. When the two-fluid theory applied to fluidisation, the solid phase is assumed to be at the onset of fluidisation. Therefore, the maximum solid volume fraction value as 0.55 is justified.

The interphase momentum transfer coefficient, K_{sg} considers the form drag and skin drag between two phases. Although more rigorous and complicated theories have been proposed for calculation of the K_{sg} values (e.g., Kandhai et al. [31]), the semi-empirical correlations had been successfully adopted in previous modelling [12–18] and were used in this work,

$$K_{sg} = \frac{3}{4} C_D \frac{\varepsilon_s \rho_g |\vec{u}_s - \vec{u}_g|}{\phi_s d_p} \varepsilon_g^{-1.65} \quad \text{for} \quad \varepsilon_g > 0.8 \tag{4}$$

$$K_{sg} = 150 \frac{(1-\varepsilon_g)^2}{\varepsilon_g} \frac{\mu_g}{\phi_s^2 d_p^2} + 1.75 \frac{\varepsilon_s \rho_g |\vec{u}_s - \vec{u}_g|}{\phi_s d_p} \quad \text{for} \quad \varepsilon_g \leq 0.8 \tag{5}$$

where the drag coefficient C_D is

$$C_D = \frac{24}{Re_s}[1 + 0.15(Re_s)^{0.687}] \quad \text{for} \quad Re_s < 1000 \tag{6}$$

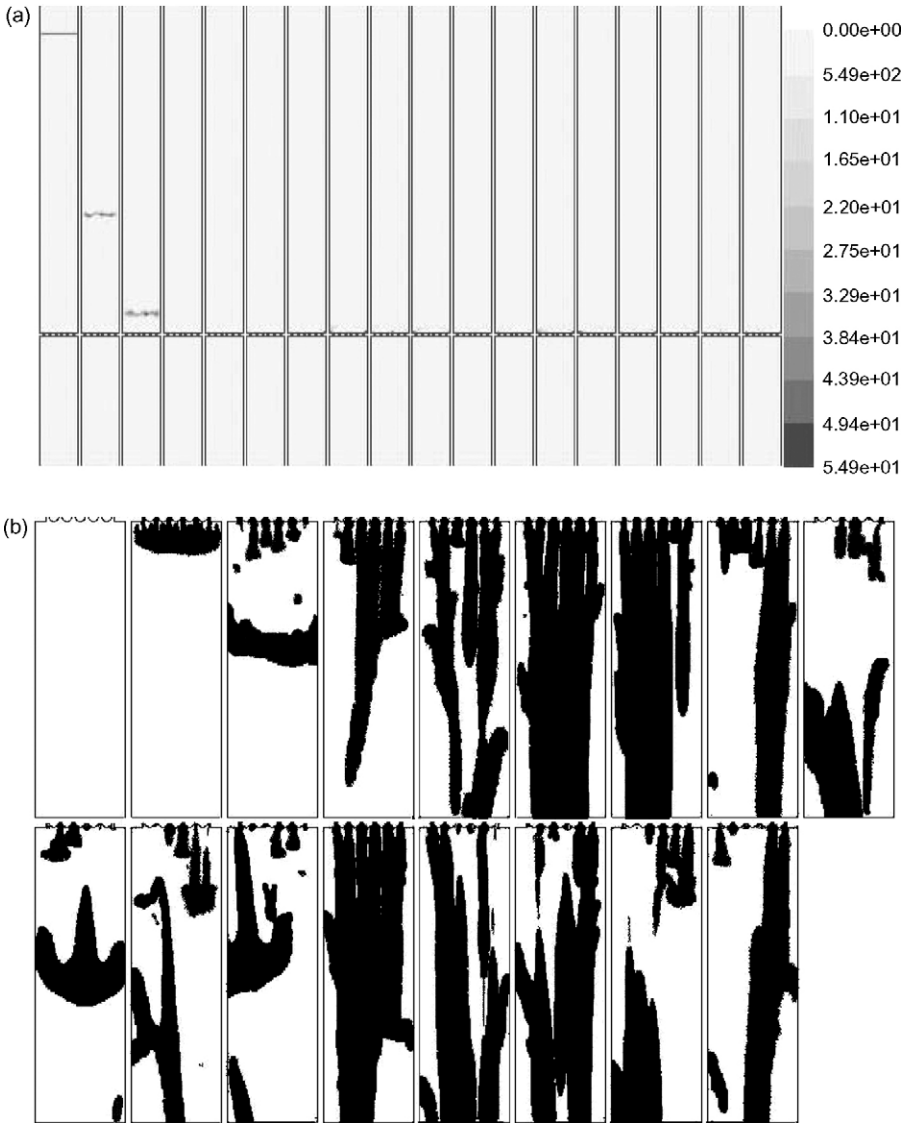

Fig. 2. (a) The snapshots of the bed at $t = 0.05$, 1.0, 1.4, 1.6, 2, 4, 10, 15, 20, 25, 30, 35, 40, 45, 50, 55, 60, 62.5 second from left to right, respectively and (b) the discharging of the solids through the distributor, at $t = 1.4$, 1.6, 2, 3, 4, 6, 9, 10, 20, 21, 24, 30, 32, 33, 34, 50, 62.5 s from left to right, top to bottom, respectively for case 1. The colour represents the solid fraction. A non-growth bed is obtained and the raining discharge mechanism is simulated.

$$C_D = 0.44 \quad \text{for} \quad Re_s \geq 1000 \tag{7}$$

and

$$Re_s = \frac{\varepsilon_g \rho_g d_p |\vec{u}_s - \vec{u}_g|}{\mu_g} \tag{8}$$

The gas phase was modelled using the modified dispersed k–ε model. The model is the standard k–ε model with an additional source term, Π_{kg}, in the turbulent kinetic energy equation and an additional source term, $\Pi_{\varepsilon g}$, in the dissipation of turbulent kinetic energy equation [32,33]:

$$\frac{\partial(\varepsilon_g \rho_g k_g)}{\partial t} + \nabla(\varepsilon_g \rho_g k_g \vec{u}_g) = \nabla(\varepsilon_g \mu_{tg} \nabla k_g) + 2\varepsilon_g \mu_{tg} E_{gs} E_{gs} - \varepsilon_g \rho_g \varepsilon_{\varepsilon g} + \Pi_{kg} \tag{9}$$

$$\frac{\partial(\varepsilon_g \rho_g \varepsilon_{\varepsilon g})}{\partial t} + \nabla(\varepsilon_g \rho_g \varepsilon_{\varepsilon g} \vec{u}_g) = \nabla(\varepsilon_g \mu_{tg} \nabla \varepsilon_{\varepsilon g}) + 2.88 \frac{\varepsilon_{\varepsilon g}}{k_g} \varepsilon_g \mu_{tg} E_{gs} E_{gs} - 1.92 \varepsilon_g \rho_g \frac{\varepsilon_{\varepsilon g}^2}{k_g} + \Pi_{\varepsilon g} \tag{10}$$

where E_{gs} is the modulus of the mean rate-of-strain tensor and

$$\mu_{tg} = 0.09 \rho_g \frac{k_g^2}{\varepsilon_{\varepsilon g}} \tag{11}$$

The additional terms Π_{kg} and $\Pi_{\varepsilon g}$ represent the influence of the dispersed solids phase on the gas phase. Following the work of Bel F'Dhila and Simonin (1992) [34],

$$\Pi_{kg} = \sum_{s=1}^{M} K_{sg} [< \vec{u}_g'' \vec{u}_s'' > + (\vec{u}_s - \vec{u}_g) \vec{v}_{dr}] \tag{12}$$

and the work of Elgobashi and Abou-Arab (1983) [35],

$$\Pi_{\varepsilon g} = 1.2 \frac{\varepsilon_{\varepsilon g}}{\varepsilon_g \rho_g k_g} \Pi_{kg} \tag{13}$$

where M represents the number of the solids phases; $\vec{u}_i''$ the fluctuating part of the local instantaneous velocity of the ith phase; $\vec{v}_{dr}$ is the drift velocity that results from turbulent fluctuations in the volume fraction and the calculations of the drift velocity can be found in [32,33].

Following the work of Hinze (1975) [36], the solids phase was modelled using the Tchen-theory of dispersion of discrete particles. Time and length scales that characterize the motion are used to evaluate dispersion coefficients, correlation functions, and the turbulent kinetic energy of the solids phase. The details can be found in [32,37].

The numerical method for the solution of this work is the finite volume method. The first order implicit method was used to estimate the scale quantity at the next time step and the second order upwind scheme was utilized to calculate the gradient terms. The enhanced wall treatment was used to solve the properties near the wall. The zone just next to the wall was treated as the viscosity-affected region and the turbulent viscosity with enhanced wall treatment was used to calculate the turbulent kinetic energy, the dissipation rate of turbulent kinetic energy, and the velocities for both phases.

A hydrodynamic model describing the gas–solid flow characteristics in the countercurrent fluidised bed was solved using the phase-coupled Semi-Implicit Method for Pressure-Linked Equation (PC-SIMPLE) algorithm programmed by the commercial software Fluent 6.1.22.

3. Simulation experiments

Fig. 1(a) shows the geometry of the simulated system: a two-dimensional countercurrent fluidised bed column with the length 350 mm and width 30 mm. The system is divided into four sections and each section is meshed into cells with different sizes. From the top of the column, the first section is 245 mm in length and 30 mm in width and is structured meshed with 0.8 mm × 0.8 mm squares; the second section is 10 mm in length and 30 mm in width and applies the unstructured meshes

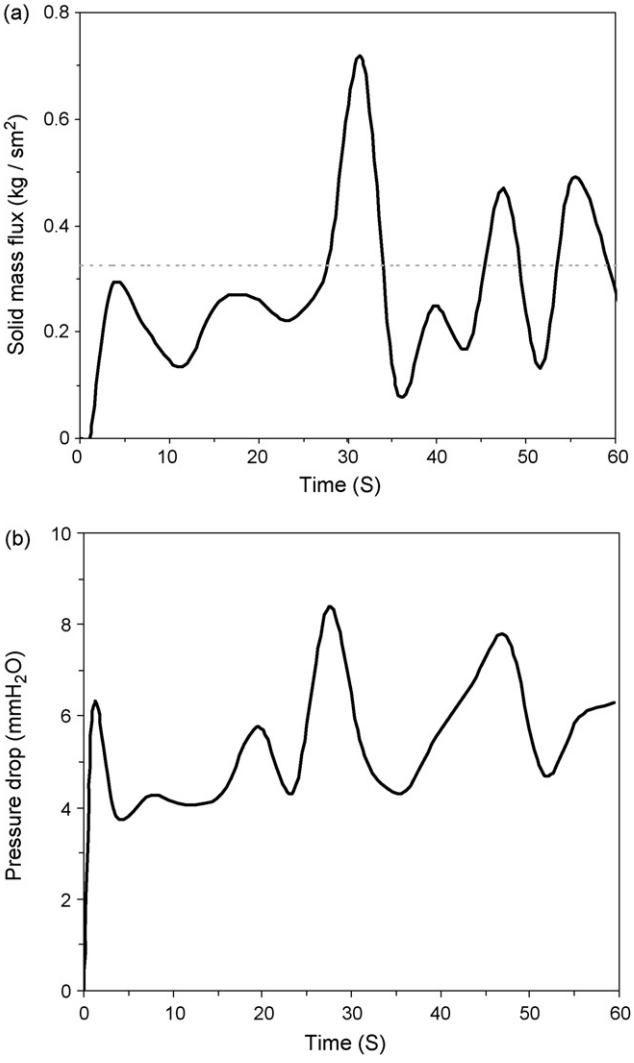

Fig. 3. (a) The simulated solid mass flux as a function of time for the case 1. The dash line indicates the solids feeding rate. (b) The simulated pressure drop across the bed as a function of time for the case 1.

with side interval 0.5 mm; the third section is 35 mm in length and 30 mm in width and applies the unstructured meshes with side interval 0.55 mm; the fourth section is 60 mm in length and 30 mm in width and is structured meshed with 0.8 mm × 0.8 mm squares. The top of the column is the outlet boundary for the gas phase and is also the inlet boundary for the solid phase. When the gas phase reaches the top of the column, it leaves the column with the velocity as it enters the column. The bottom of the column serves as the inlet boundary for gas phase and also as the outlet boundary for the solid phase. When the solid phase reaches the bottom of the column, it accelerates leaving the column with an arbitrary chosen velocity 100 m/s. A dual flow distributor is located at a height 100 mm above the bottom of the column and the geometry of the distributor is shown in Fig. 1(b). The linear opening ratio of the distributor is 20%.

In order to compare our simulation results with the experimental work of Kuo and Cheng [22], carborundum particles and air with a temperature 293 K, density 1.2074 kg/m^3 and viscosity 1.787×10^{-5} kg/ms are selected as the two phases in the simulations. Particles with a mean diameter 335 μm, density 3150 kg/m^3 are the "solid phase" in the simulations. Goldschmidt et al. [14] and Du et al. [6] showed that the restitution coefficient had a significant impact of the fluidization behaviour

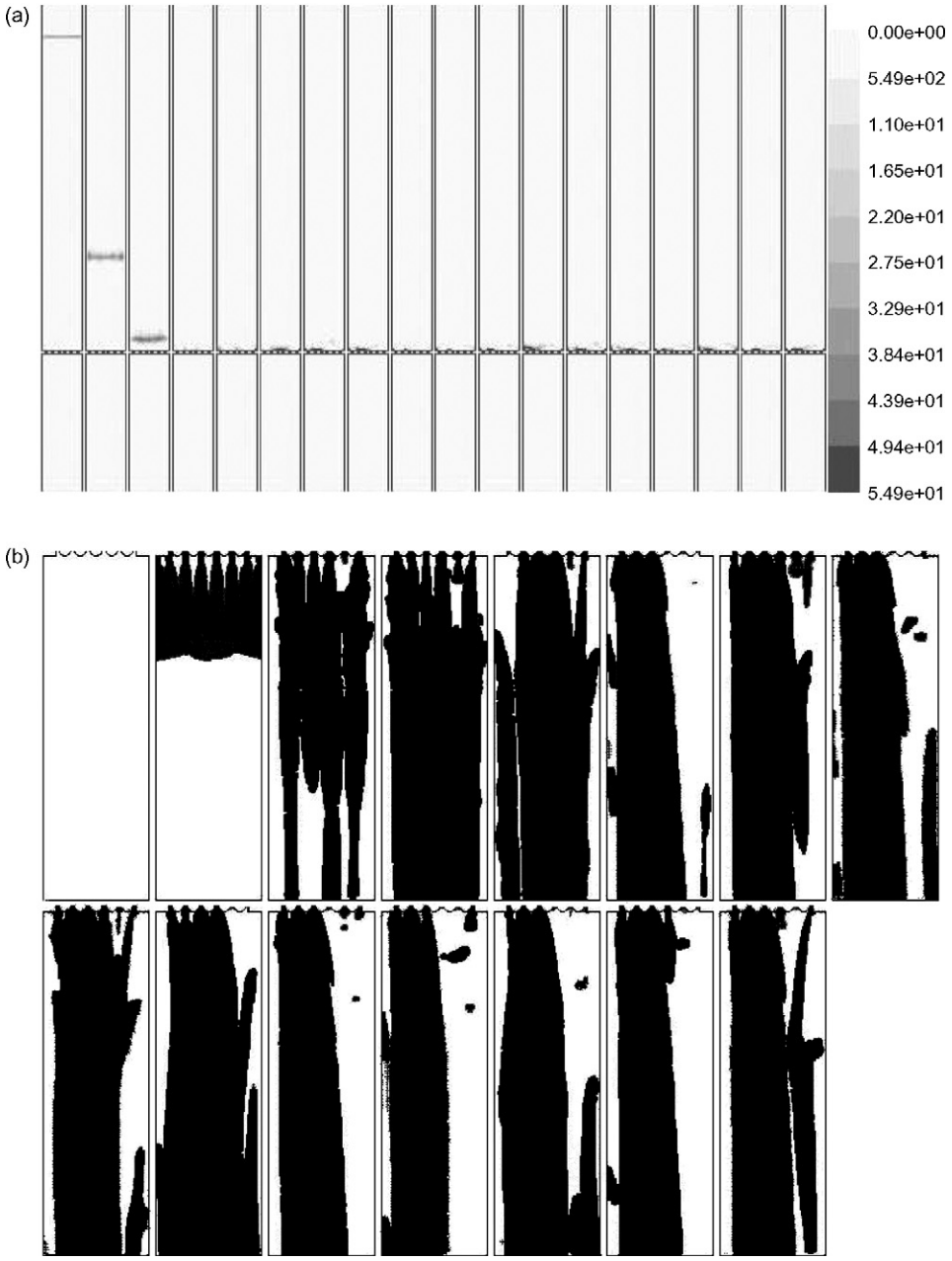

Fig. 4. (a) The snapshots of the bed at $t = 0.05$, 0.8, 1.0, 2.6, 4, 5, 10, 15, 20, 25, 30, 35, 40, 45, 50, 55, 60, 72 s from left to right, respectively and (b) the discharging of the solids through the distributor at $t = 1.0$, 1.2, 2.4, 2.6, 5, 10, 20, 30, 40, 45, 50, 55, 60, 70, 72 s from left to right, top to bottom, respectively for case 2. The colour represents the solid fraction. A dilute bed is obtained and the raining and dumping discharge mechanisms are simulated.

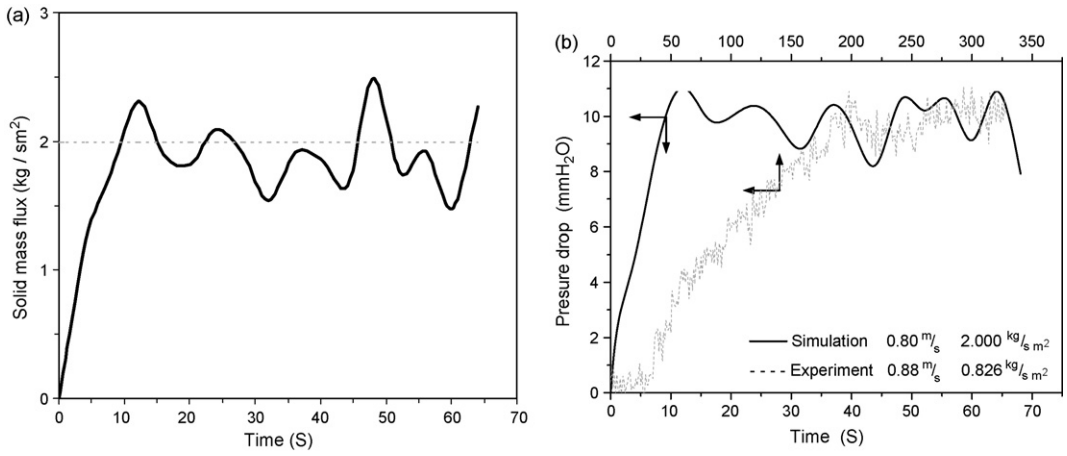

Fig. 5. (a) The simulated solid mass flux as a function of time for the case 2. The dash line indicates the solids feeding rate. (b) The simulated pressure drop across the bed as a function of time for the case 2 together with the experimental results of [22].

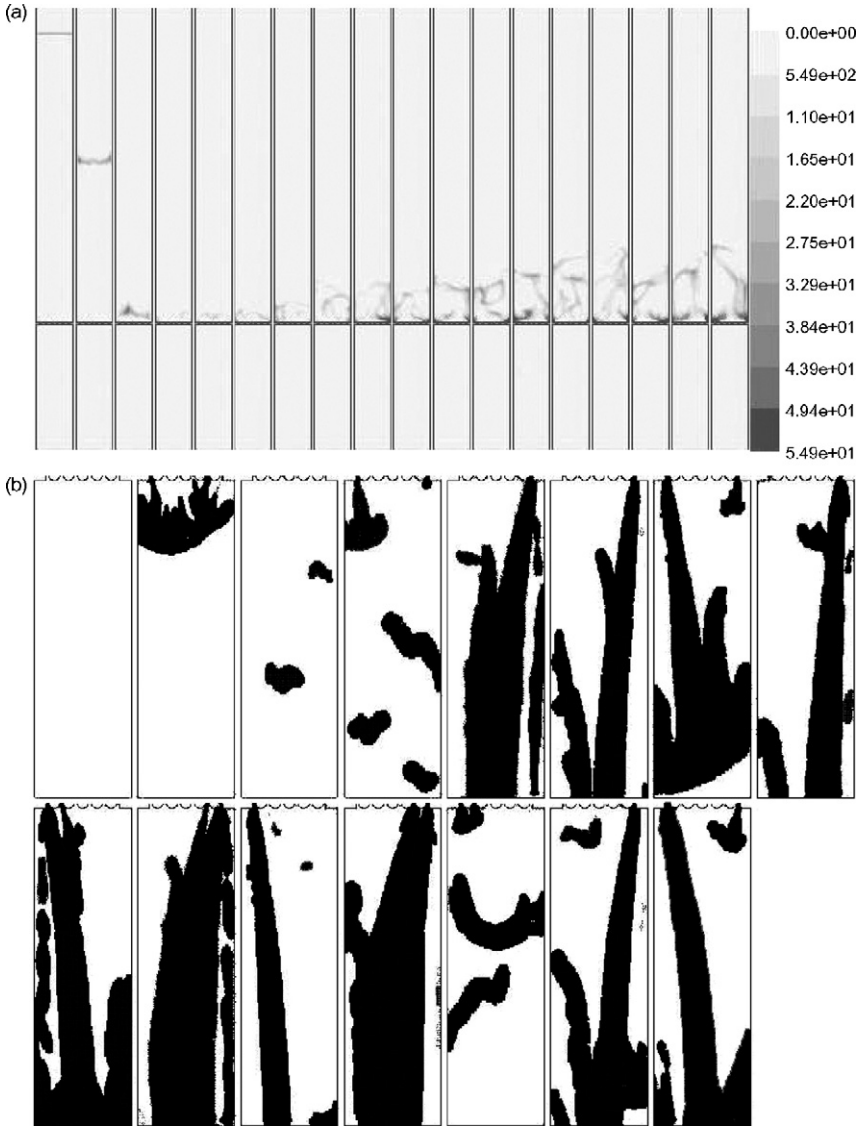

Fig. 6. (a) The snapshots of the bed at $t = 0.05$, 1.0, 1.8, 2.6, 3, 5, 7, 10, 13, 16.05, 20.05, 25.05, 30.05, 35.05, 40.05, 45.05, 50.05, 61.05 s from left to right, respectively and (b) the discharging of the solids through the distributor at $t = 1.8$, 2.2, 6, 10, 14, 17.05, 21.05, 25.05, 31.05, 37.05, 42.05, 45.05, 48.05, 54.05, 61.85 s from left to right, top to bottom, respectively for case 5. The colour represents the solid fraction. An oscillating bed is obtained and the circulating dumping discharge mechanism is simulated.

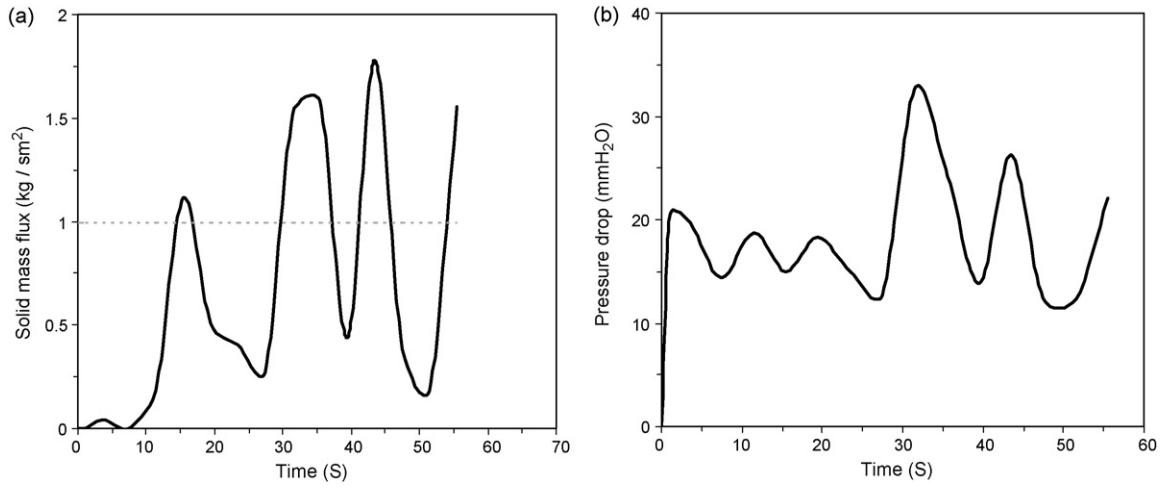

Fig. 7. (a) The simulated solid mass flux as a function of time for the case 5. The dash line indicates the solids feeding rate. (b) The simulated pressure drop across the bed as a function of time for the case 5.

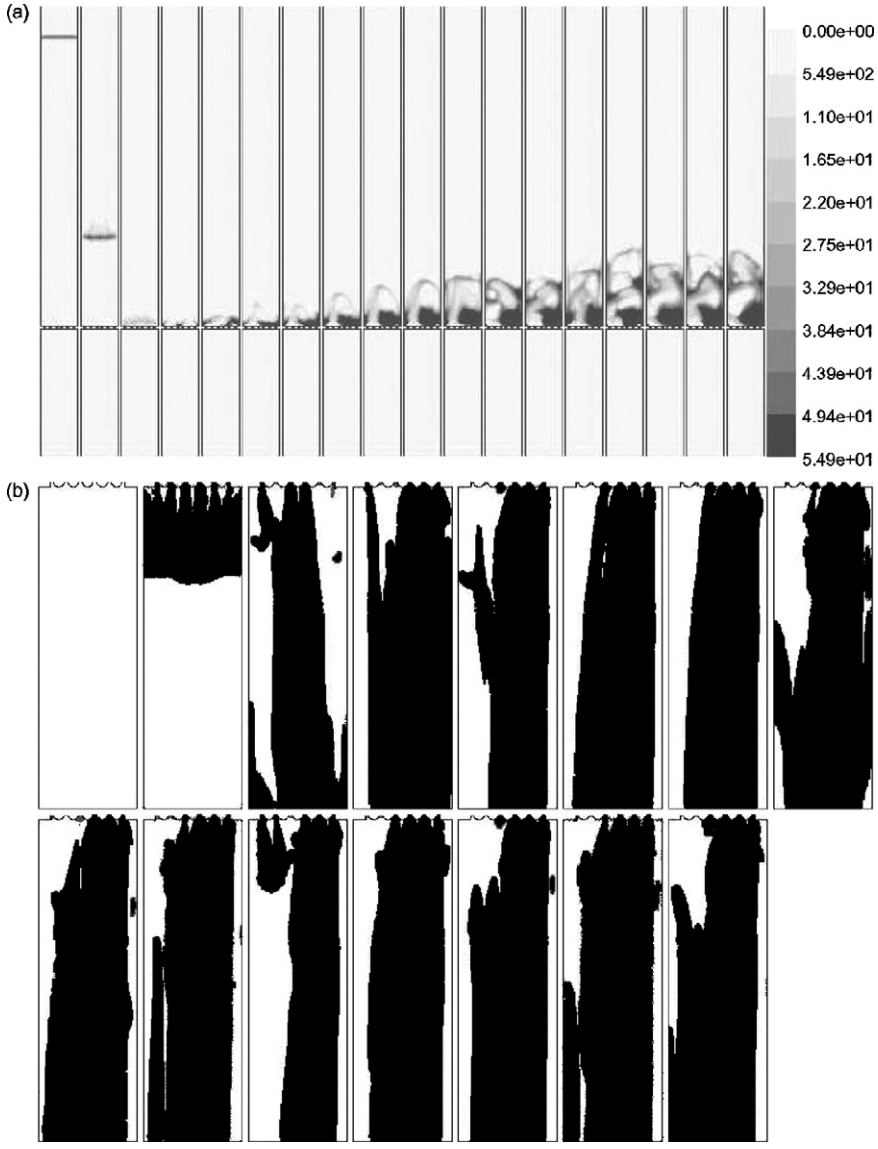

Fig. 8. (a) The snapshots of the bed at $t = 0.05$, 0.8, 1.0, 3, 5, 7, 10, 13, 16, 20.05, 25.05, 30.05, 35.05, 40.05, 45.05, 50.05, 55.05, 62.05 s from left to right, respectively and (b) the discharging of the solids through the distributor at $t = 1.0$, 1.2, 2, 6, 10, 15, 20.05, 25.05, 30.05, 35.05, 40.05, 45.05, 50.05, 55.05, 62.05 s from left to right, top to bottom, respectively for case 6. The colour represents the solid fraction. A stable bubbling bed is obtained and the dumping discharge mechanism is simulated.

and its value should be carefully selected according to the material properties. The restitution coefficient of particles as hard as carborundum is around 0.9. Therefore, in the following computations, e_{ss} equals to 0.9 was used. Table 2 shows the 13 operation conditions (i.e., the solids feeding flux and gas velocity as the initial conditions) simulated in the current study. The calculation of the simulation parameter values listed in Table 2 is given in the Appendix.

At the beginning of each simulated case, the calculation time step was 5×10^{-5} second. After *ca.* 2.5–2.8 s simulation time, the calculation residual reached a steady value and the time step was increased to 1×10^{-4} s to accelerate the calculation CPU time. The computing facility used was Intel(R) Xeon(TM) running at 2.80 GHz.

4. Results and discussion

Gas/solid pressure, gas/solid velocities, and gas/solid fraction in each cell are calculated at every time step and therefore massive information is obtained. Two schemes were adopted to present our simulation results, which are the snapshots of the whole system at selected times in a macroscopic viewpoint and the calculated values in the selected cells of the system at selected times in a microscopic viewpoint. We carefully choose three levels of the column (see Fig. 1(a)) to present data in the microscopic fashion. The lowest level A is located 5 mm above the bottom of the column. The discharge of the solids can be characterized at this level. Level B is 5 cm above the bottom of the column and level C is 5 mm below the top of the column. Levels B and C are selected to locate above and below the bed so that the pressure across the bed can be calculated and hence can be compared with the experimental measurements of [22].

4.1. The flow regimes

From previous experimental studies, there are five bed regimes in a countercurrent fluidised bed on a dual flow distributor at different operation conditions, including a non-growth bed, a dilute bed, an oscillating bed, a stable bubbling bed and a flooding bed [21]. Since the 2D simulated system is geometrically similar to the 3D system of Kuo and Cheng [22] and the same particle properties are used in both systems, we compare our simulated results with their experimental measurements.

A typical result of the non-growth bed is obtained using the simulation parameters of case 1 and snapshots of the simulation results at different times are shown in Fig. 2(a). Since the particles are fed continuously into the column from the top of the column, the particles form cluster when they first encounter with the gas as shown at time 0.05, 1.0 and 1.4 s. No appreciate particles are accumulated on the distributor. Therefore, a non-growth bed is obtained. A different scale of the level of the contour plot was selected to study the discharging mechanisms in a non-growth bed at different times and the results are shown in Fig. 2(b). After the solid cluster strikes the distributor, the particles fall into the wind-box via a raining mechanism are well simulated. The raining discharging mechanism occurs when the inertia of a dropped particle is greater than the summation of the drag and the buoyancy forces acting on it, and the particle happens to drop through the holes of the distributor, the particles fall into wind-box individually [21].

The solids mass flux of each cell at level A was averaged every 4 s and the result for case 1 is shown in Fig. 3(a). The solid mass flux at level A (i.e., the solids discharging rate) at steady state is *ca.* 0.328 kg/sm^2 (the dash line), which is the same as the value of the solids feeding rate. For a bed to growth, one may expect that the solids discharging rate is smaller than the solids feeding rate. In case 1, there is limited time duration that the solids discharging rate is smaller than solids feeding rate; therefore, a non-growth bed is obtained. Fig. 3(b) represents the pressure drop across the bed as a function of the simulation time for case 1. The pressure drop across the bed is approximately 5.3 mmH_2O at steady state. In the experiments of [22], the pressure drop across a non-growth bed is as low as few mmH_2O. Our simulation result agrees quantitatively well with the experimental measurements.

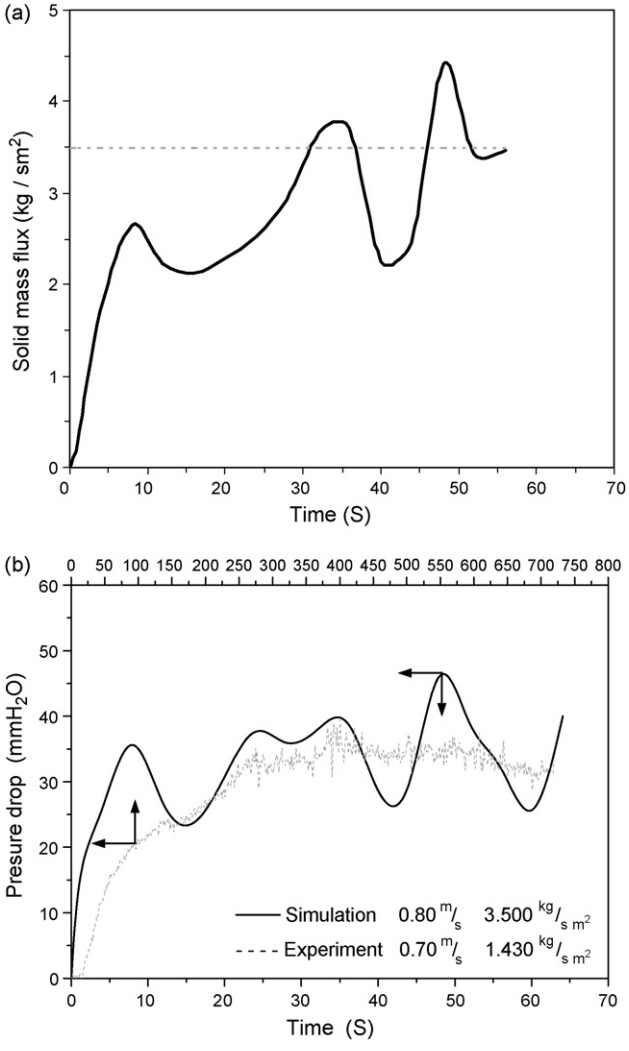

Fig. 9. (a) The simulated solid mass flux as a function of time for the case 6. The dash line indicates the solids feeding rate. (b) The simulated pressure drop across the bed as a function of time for the case 6 together with the experimental results of [22].

A typical dilute flow regime is obtained using the simulation parameters of case 2 and snapshots of the simulation results at different times are shown in Fig. 4(a). There are small amounts of particles accumulated above the plate after the cluster encounters the plate and result in the formation of a dilute bed. The snapshots of the discharge of solids as a function of time are shown in Fig. 4(b). The raining discharging mechanism only exists at a short period after the cluster encounters the plate. After 2.4 s, the dumping mechanism appears to be the main discharging mechanism. Fig. 5(a) shows the solids discharging rate for case 2 and the dash line represents the solids feeding rate. The discharge of solids increases at the first 10 s and reaches an approximate steady value of 2.0 kg/sm^2, which is the same value as the feeding rate of the solids in case 2. Thus, limited particles accumulated above the plate in the first 10 s cause the formation of a dilute bed. The pressure drop across the bed as a function of the simulation time is shown in Fig. 5(b), together with the experimental results of [22]. In both simulation prediction and experimental observation, the pressure drop across the bed at steady state is approximately 10 mmH_2O. A quantitative agreement is obtained, although the solids feeding rate and the time to reach the steady state are different. The differences in the time to steady state are probably due to the fact that the 2D simulation results are compared

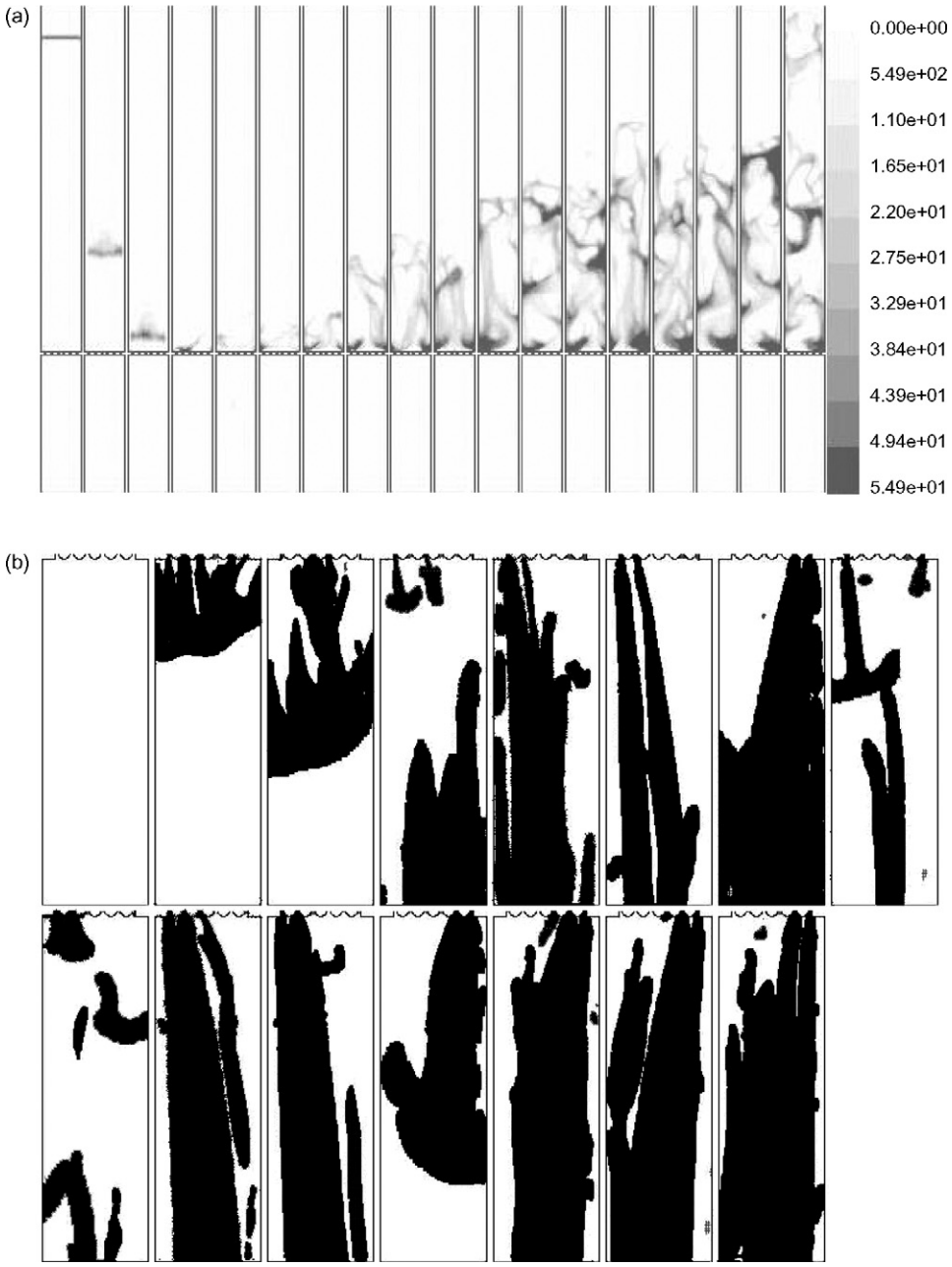

Fig. 10. (a) The snapshots of the bed $t = 0.05$, 1.0, 1.4, 1.6, 2, 3, 5, 10, 13, 16, 20, 23, 26, 30, 31, 32, 33, 34 s from left to right, respectively and (b) the discharging of the solids through the distributor at $t = 1.4$, 1.8, 2.2, 3, 6, 10, 12, 16, 17, 20, 25, 29, 31, 32, 34 s from left to right, top to bottom, respectively for case 11. The colour represents the solid fraction. A flooding bed is obtained and the weeping and dumping discharge mechanisms are simulated.

with the 3D experimental results and the opening of the plate (see later).

The snapshots of the simulation results at different times for case 5 are shown in Fig. 6(a). An oscillating bed is observed. The main characteristic of an oscillating bed is the circulating dumping of the particles around the plate [21] and this is well simulated in Fig. 6(b). The particles are discharged as a group through the left half and the right half of the plate in turns. The circulating dumping of the solids into the wind-box is also shown in Fig. 7(a). The fluctuations in Fig. 7(a) are resulted from the circulating dumping of an oscillating bed. An average discharging rate of 1.0 kg/sm^2 is the same as the solids feeding rate after 30 s, causing the number of the particles above the plate remains an approximate constant amount. The pressure drop across the bed of case 5 is shown in Fig. 7(b). The pressure drop oscillates and the average value after 30 s is *ca.* 18 mmH_2O. Although the pressure drop across an oscillating bed depends on the characteristics of the particles and the plate design, the value of the pressure drop across an oscillating the bed at steady state is between that of a dilute bed at steady state and a stable bed at steady state [21]. The calculated pressure drop across the oscillating bed agrees qualitatively with the experimental investigation.

The snapshots of the simulation results at different times for case 6 are shown in Fig. 8(a). A stable bed is formed at steady state. Fig. 8(b) shows the snapshots of the discharging of solids at different times. The dumping of solids in a bubbling bed is due to the eruption of the bubbles at the surface of the bed and the particles slosh towards the plate, forcing a group of particles to fall into the wind-box [21]. Such a dumping mechanism is predicted in the current simulation. In Fig. 9(a) and (b), the discharge of solids and the pressure drop across the bed fluctuates due to the dumping of the solids into the wind-box periodically. The pressure drop across the bed at steady state is approximately 35 mmH_2O. In the experiments of [22], the pressure drop across a stable bubbling bed is between 10 and 35 mmH_2O. Our simulation results agree quantitatively well with the experimental results in the stable pressure drop. The differences in the time to steady state are probably due to the fact that the 2D simulation results are compared with the 3D experimental results and the opening of the plate (see later).

In case 11, a flooding bed is obtained and the snapshots of the system at different times are shown in Fig. 10(a). Similar to the experimental observations of [21,22], large slugs are formed in the system. The particles discharge into the wind-box via the weeping and dumping mechanisms (Fig. 10(b)). With a weeping mechanism, particles fall into the wind-box from the periphery of the holes individually and the rate of solids discharging decreases. Therefore, the discharging of solids is slower the solids feeding rate (also shown in Fig. 11(a) and the particles finally flood out of the system. Fig. 11(b) shows the pressure drop across the bed as a function of time. Because of the accumulation of the particles above the plate, the pressure drop increases monotonically, which agrees well with the experimental result of [22].

Fig. 12(a) and (b) are flow regimes as functions of the solid mass flux and the gas velocity from the experimental observation

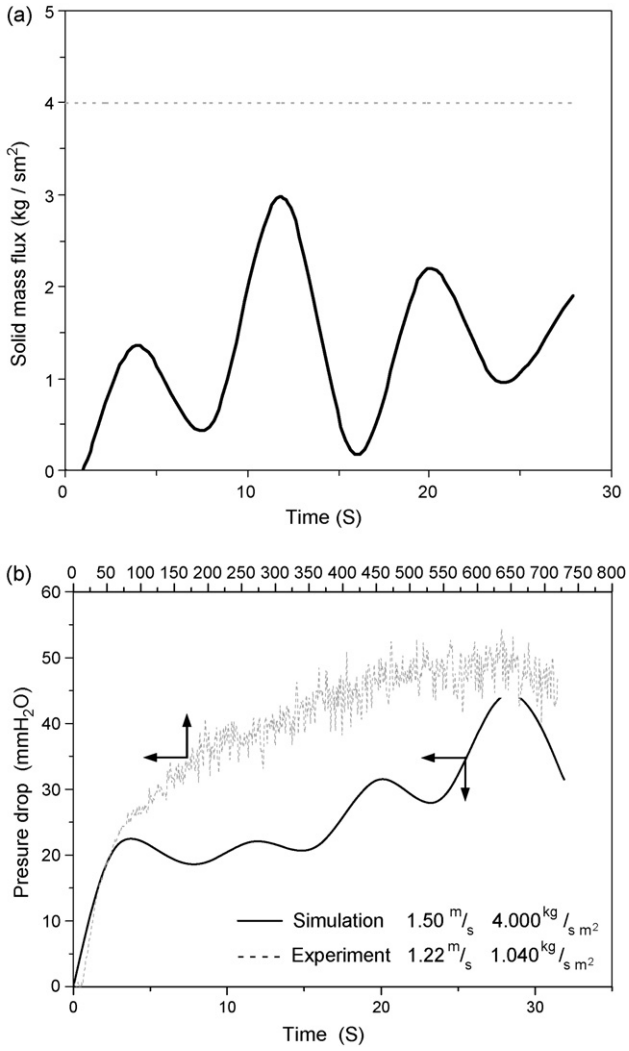

Fig. 11. (a) The simulated solid mass flux as a function of time for the case 11. The dash line indicates the solids feeding rate. (b) The simulated pressure drop across the bed as a function of time for the case 11 together with the experimental results of [22].

[22] and the CFD simulation, respectively. In both cases, the flow regime changes from a non-growth bed, a dilute bed, a stable bubbling bed to a flooding bed with the increase of the solids feeding rates and/or the gas velocities. When comparing the stable operation range of such a system, the 2D simulated results agree qualitatively with the 3D experimental data.

In all the above comparisons, we find that the five types flow regimes, the pressure drop across the bed at steady state for the dilute and stable beds, and the flow regimes as functions of the solids feeding rate and the gas velocities are well simulated. However, the solids feeding rates are very different from the experimental prediction and the experimental observation of [22]. The deviations are probably due to the following two reasons. Firstly, a two-dimensional simulation has been used to predict the behaviour of a three-dimensional system. The motion of the particles and the gas has been restricted in the simulation compared with the experimental investigation. Secondly, the distributor may cause such a deviation. The opening ratio of a two-dimensional system is the *length* of the opening holes

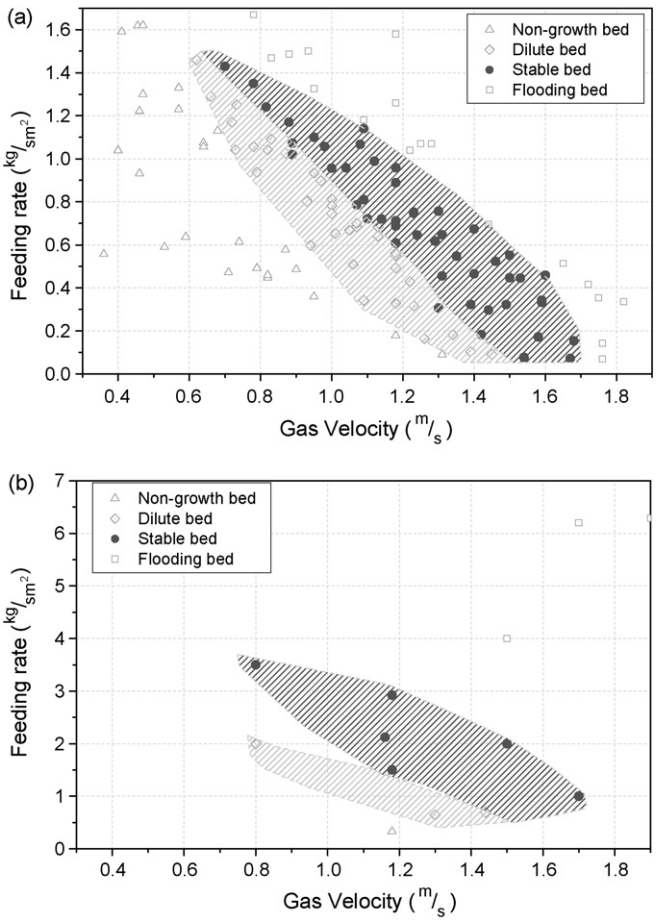

Fig. 12. The comparison of the flow regimes as functions of the solid feeding velocity and gas velocity between of the (a) experimental results of [22] and (b) simulation results.

divided by the column width, while the opening ratio of a three-dimensional system is the *area* of the opening holes divided by the cross-section area of the column. The plane through the cylindrical column along its height is simulated in this work. Although the linear open ratio of the distributor in the simulation is the same as that in the experiments, the numbers of the holes are different when one fixed the opening ratio constant. The difference in the number of the hole affect the gas velocity through the hole and therefore the deviation of the current simulation results from the experimental investigation is possible, although we have made the closest approach to the real system.

5. Conclusion

An Eulerian–Eulerian approach coupled with kinetic theory of granular flow (KTGF) for the solid phase Computation Fluid Dynamics (CFD) method was applied to study a countercurrent staged fluidised bed. The non-growth bed, the dilute bed, the oscillating bed, the stable bubbling bed, the flooding beds were modelled as different operating conditions. The predicted pressure drops across the bed in different beds agree quantitatively well with the experimental results of Kuo and Cheng [22].

The microscopic study on the discharging mechanism agrees with the experimental observation of Ju et al. [21]: the raining mechanism is the major discharging mechanism in a non-growth bed; the circulating dumping mechanism is the major discharging mechanism in an oscillating bed; the weeping mechanism is the major discharging mechanism in a flooding bed and the bubble erupting dumping mechanism is the major discharging mechanism in dilute and stable bubbling beds. The flow regime changes from a non-growth bed, a dilute bed, a stable bubbling bed to a flooding bed with the increase of the solids feeding rates and/or the gas velocities in both our simulations and previous experimental results. When comparing the stable operation range of such a system, the 2D simulated results agree qualitatively with the 3D experimental data. Nevertheless, we demonstrated that CFD is capable to catch both the macroscopic and microscopic behaviour of the system and predicted quantitatively well in the values of the pressure drop across the bed for the dilute flowing regime and the bubbling flowing regime at steady state, which are probably one of the most important operation parameters in real operations.

Acknowledgement

The authors are grateful for the financial support from National Science Council of the Republic of China (NSC92-2212-E-182-006).

Appendix A. Calculation of the simulation parameter at boundaries

The feeding velocity, the solids fraction and the granular temperature of the particle phase at the inlet are required for the simulation. In the experiment of [22], the feeding of solids is $h = 0.139$ m above the top of the column. The particle phase inlet velocity is,

$$\vec{u}_s = \sqrt{2\vec{g}h} = 1.65\,\mathrm{m/s} \tag{A.1}$$

The solids fraction in the particle phase can be obtained from the solids feeding mass flux, $\dot{m}$, the density of the solid phase, ρ_s, and the particle phase velocity, $\vec{u}_s$ as

$$\varepsilon_s = \frac{\dot{m}}{\rho_s \vec{u}_s} \tag{A.2}$$

The granular temperature is [16],

$$\theta_s = 0.004(u_s)^2 \tag{A.3}$$

Because the gas phase is modelled as a turbulent phase and the k–ε model is used to model the turbulent kinetic energy of the gas phase, two simulation parameters for the turbulence are required.

The turbulent kinetic energy of the inlet gas is obtained by [16],

$$k = 0.004(\vec{u}_g)^2 \tag{A.4}$$

where $\vec{u}_g$ is the inlet gas velocity, and the turbulent dissipation rate is,

$$\varepsilon' = 2\frac{k^{0.75}}{\kappa d} \tag{A.5}$$

where κ is the von Kármán constant and d is the diameter of the fluidized bed.

References

[1] M. Stein, Y.L. Ding, J.P.K. Seville, Experimental verification of the scaling relationships for bubbling gas-fluidised beds using the PEPT technique, Chem. Eng. Sci. 57 (2002) 3649–3658.

[2] P.S. Fennell, J.F. Davidson, J.S. Dennis, L.F. Gladden, A.N. Hayhurst, M.D. Mantle, C.R. Müller, A.C. Rees, S.A. Scott, A.J. Sederman, A study of the mixing of solids in gas-fluidized beds, using ultra-fast MRI, Chem. Eng. Sci. 60 (2005) 2085–2088.

[3] J.J.N. Alves, M. Mori, Fluid dynamic modelling and simulation of circulating fluidized bed reactors: analyses of particle phase stress models, Comput. Chem. Eng. 22 (1998) S763–S766.

[4] S. Benyahia, H. Arastoopour, T.M. Knowlton, H. Massah, Simulation of particles and gas flow behavior in the riser section of a circulating fluidized bed using the kinetic theory approach for the particulate phase, Powder Technol. 112 (2000) 24–33.

[5] D.J. Patil, M. van Sint Annaland, J.A.M. Kuipers, Critical comparison of hydrodynamic models for gas–solid fluidized beds. Part I: bubbling gas–solid fluidized beds operated with a jet, Chem. Eng. Sci. 60 (2005) 57–72.

[6] W. Du, X.J. Bao, J. Xu, W.S. Wei, Computational fluid dynamics (CFD) modeling of spouted bed: influence of frictional stress, maximum packing limit and coefficient of restitution of particles, Chem. Eng. Sci. 61 (2006) 4558–4570.

[7] T. Kawaguchi, M. Sakamoto, T. Tanaka, Y. Tsuji, Quasi-three-dimensional numerical simulation of spouted beds in cylinder, Powder Technol. 109 (2000) 3–12.

[8] T. Kawaguchi, T. Tanaka, Y. Tsuji, Numerical simulation of two-dimensional fluidized beds using the discrete element method (comparison between the two- and three-dimensional models), Powder Technol. 96 (1998) 129–138.

[9] C.X. Chen, L.S. Fan, Discrete simulation of gas–liquid bubble columns and gas–liquid–solid fluidized beds, AIChE J. 50 (2004) 288–301.

[10] C.K.K. Lun, S.B. Savage, D.J. Jeffrey, Kinetic theories for granular flow: inelastic particles in couette flow and slightly inelastic particles in general flow field, J. Fluid Mech. 140 (1984) 223–256.

[11] J.A.M. Kuipers, A two-fluid micro balance model of fluidized bed, Ph.D. Thesis, Twente University, Enschede, The Netherlands, 1990.

[12] I.K. Gamwo, Y. Soong, R.W. Lyczkowski, Numerical simulation and experimental validation of solids flows in a bubbling fluidized bed, Powder Technol. 103 (1999) 117–129.

[13] S.J. Zhang, A.B. Yu, Computational investigation of slugging behaviour in gas-fluidised beds, Powder Technol. 123 (2002) 147–165.

[14] M.J.V. Goldschmidt, J.A.M. Kuipers, W.P.M. van Swaaij, Hydrodynamic modelling of dense gas-fluidised beds using the kinetic theory of granular flow: effect of coefficient of restitution on bed dynamics, Chem. Eng. Sci. 56 (2001) 571–578.

[15] E. Peirano, B. Leckner, Fundamentals of turbulent gas–solid flows applied to circulating fluidized bed combustion, Prog. Energy Combust. Sci. 24 (1998) 259–296.

[16] Y. Zheng, X.T. Wan, Z. Qian, F. Wei, Y. Jin, Numerical simulation of the gas–particle turbulent flow in riser reactor based on k–ε–k_p–ε_p–θ two-fluid model, Chem. Eng. Sci. 56 (2001) 6813–6822.

[17] L. Huilin, D. Gidaspow, Hydrodynamics of binary fluidisation in a riser: CFD simulation using two granular temperatures, Chem. Eng. Sci. 58 (2003) 3777–3792.

[18] A.K. Das, J.D. Wilde, G.J. Heynderickx, G.B. Marin, J. Vierendeels, E. Dick, CFD simulation of dilute phase gas–solid riser reactors: part I. A new solution method and flow model validation, Chem. Eng. Sci. 59 (2004) 167–186.

[19] R. Toei, T. Akao, Multi-stage fluidised bed apparatus with perforated plates, IChemE Symp. Ser. 30 (1968) 34–42.

[20] D. Gauthier, G. Flamant, Residence time distribution in a series of three tanks with bypass and back-mixing. Application to multistage fluidised-bed, Chem. Eng. Commun. 100 (1991) 77–94.

[21] S.P. Ju, W.M. Lu, H.P. Kuo, F.S. Chu, Y.C. Lu, The formation of a suspension bed on dual flow distributors, Powder Technol. 131 (2003) 139–155.

[22] H.P. Kuo, C.Y. Cheng, Investigation of the bed types and particle residence time in a staged fluidised bed, Powder Technol. 169 (2006) 1–9.

[23] H.P. Kuo, M.L. Ku, On the plate design in a countercurrent single-stage fluidized bed system, Adv. Powder Technol 19 (1) (2008), in press.

[24] J. Ding, D. Gidaspow, A bubbling fluidisation model using kinetic theory of granular flow, AIChE J. 36 (1990) 523–538.

[25] S. Ogawa, A. Umemura, N. Oshima, On the equations of fully fluidized granular materials, J. Appl. Math. Phys. 31 (1980) 483–493.

[26] R.M. German, Particle Packing Characteristics, Princeton, New Jersey, 1989.

[27] A. Samuelsberg, B.H. Hjertager, An experimental and numerical study of flow patterns in a circulating fluidized bed reactor, Int. J. Multiphase Flow 22 (1996) 575–591.

[28] M. Syamlal, T.J. O'Brien, Computer simulations of bubbles in a fluidised bed, AIChE Symp. Ser. 85 (1985) 22–31.

[29] D. Gidaspow, R. Bezburuah, J. Ding, Hydrodynamics of circulating fluidised beds, kinetic theory approach, in: Fluidisation VII, Proceedings of the 7th Engineering Foundation Conference on Fluidisation, 1992, pp. 75–82.

[30] V. Mathiesen, T. Solberg, B.H. Hjertager, Predictions of gas/particle flow with an Eulerian model including a realistic particle size distribution, Powder Technol. 112 (2000) 34–45.

[31] D. Kandhai, J.J. Derksen, H.E.A. van den Akker, Interphase drag coefficients in gas–solid flows, AIChE J. 49 (2003) 1060–1065.

[32] Fluent 6.1 Documentation, Fluent Inc., 2003.

[33] R.S. Oey, R.F. Mudde, L.M. Portela, H.E.A. van den Akker, Simulation of a slurry airlift using a two-fluid model, Chem. Eng. Sci. 56 (2001) 673–681.

[34] R. Bel F'Dhila, O. Simonin, Eulerian predictions of a turbulent bubbly flow down-stream a sudden pipe expansion, in: M. Sommerfeld (Ed.), Proceedings of the 6th Workshop on Two-Phase Flow Predictions, 1992, pp. 264–273.

[35] S. Elgobashi, T. Abou-Arab, A two-equation turbulence model for two-phase flows, Phys. Fluid. 26 (4) (1983) 931–938.

[36] J.O. Hinze, Turbulence, 2nd ed., McGraw-Hill, New York, 1975.

[37] W. Du, X.J. Bao, J. Xu, W.S. Wei, Computational fluid dynamics (CFD) modeling of spouted bed: assessment of drag coefficient correlations, Chem. Eng. Sci. 61 (2006) 1401–1420.